Geophysical Research Letters

Supporting Information for

New insights into the relationship between mass eruption rate and volcanic column height based on the IVESPA dataset

Thomas J. Aubry[1,2]*, Samantha Engwell[3]*, Costanza Bonadonna[4], Larry G. Mastin[5], Guillaume Carazzo[6], Alexa R. Van Eaton[5], David E. Jessop[6,7], Roy G. Grainger[8], Simona Scollo[9], Isabelle A. Taylor[8], A. Mark Jellinek[10], Anja Schmidt[11,12,13], Sébastien Biass[4], Mathieu Gouhier[7]

*Co-first authors: these authors contributed equally to the publication.
[1]Department of Earth and Environmental Sciences, University of Exeter, Penryn, UK
[2]Previously at: Sidney Sussex College, University of Cambridge, Cambridge UK
[3]British Geological Survey, The Lyell Centre, Edinburgh
[4]Department of Earth Sciences, University of Geneva, Geneva, Switzerland
[5]U.S. Geological Survey, Cascades Volcano Observatory, Vancouver, Washington, USA
[6]Université de Paris Cité, Institut de physique du globe de Paris, CNRS, F-75005 Paris, France
[7]Université Clermont Auvergne, CNRS, IRD, OPGC Laboratoire Magmas et Volcans, F-63000 Clermont-Ferrand, France
[8]COMET, Atmospheric, Oceanic and Planetary Physics, University of Oxford, Oxford, OX1 3PU, UK
[9]Istituto Nazionale di Geofisica e Vulcanologia, Observatorio Etneo, Catania, Italy
[10]Earth Ocean and Atmospheric Sciences, University of British Columbia, Vancouver, Canada
[11]Institute of Atmospheric Physics (IPA), German Aerospace Center (DLR), Oberpfaffenhofen, Germany
[12]Meteorological Institute, Ludwig Maximilian University of Munich, Munich, Germany
[13]Department of Chemistry, University of Cambridge, Cambridge, UK

Contents of this file

Additional Supporting Information (Files uploaded separately)

Table S1. Data used in our study. Most parameters are directly taken from IVESPA version 1.0 (see https://ivespa.co.uk). Explanation on the other parameters is provided in supporting information S1-S2.

Table S2. Data compiled for isopleth height $H_{iso,top}$ estimates for IVESPA events.

Table S3. Data for empirical fits presented in Figure 1, including best fit relationships, and predictions and uncertainties for a range of $\overline{H}_{top}$ and $\overline{MER}$ values. The first sheet provides details on the following eight sheets, each of which is associated with a specific empirical fit

(four types of height, and either power law fit with $\overline{MER}$ as independent variable or log-linear fit with $\overline{H}_{top}$ as independent variable).

Introduction

This supporting information file provides details on all data derived from but not explicitly included in the IVESPA archive (S1) as well as isopleth-based height (S2). It also provides information on the analytical relationships considered in Table 1 (S3) and the fitness metrics used to compare them (S4). Figure S1-S8 mostly provide sensitivity tests on the calibration of the $\overline{H}_{top}$ - $\overline{MER}$ empirical fits, or on the dependence of the $\overline{H}_{top}$ residuals on atmospheric and eruption source parameters. This file also provides caption of additional supporting information tables (all in .xlsx format) which contain all the data used in our study (Table S1-S2) as well as information and data on all empirical fits presented in Figure 1 (Table S3).

S1. Additional parameters not explicitly provided in IVESPA

Mass eruption rate uncertainty

We define the $\overline{MER}$ as the mass of tephra fallout divided by eruption duration. For the former parameter, we only used estimates derived from mapping of the tephra fallout deposits and empirical fitting of the thinning trends. In IVESPA, unlike other parameters like height and duration, we allowed for different values of lower and upper bound uncertainty for the mass of tephra fallout because this parameter commonly shows strongly asymmetric probability distributions for its true value (Bonadonna et al., 2015c). Accordingly, in this study, we also provide a lower and upper bound uncertainty for $\overline{MER}$ which are calculated as:

$$\left(\frac{\Delta\overline{MER}_{l,u}}{\overline{MER}}\right)^2 = \left(\frac{\Delta M_{l,u}}{M}\right)^2 + \left(\frac{\Delta D}{D}\right)^2 \qquad (S.1)$$

Where Δ refers to the uncertainty, l and u subscript to the lower or upper bound uncertainty, and M and D are the mass of tephra fallout and duration, respectively.

Furthermore, we did not systematically assign an uncertainty to the mass of tephra fallout because uncertainty information on TEM in the published record is commonly not provided and hard to infer from contextual information. Accordingly, we do not attribute a $\overline{MER}$ uncertainty for events that do not have a tephra fallout mass uncertainty.

Atmospheric parameters

IVESPA contains time-averaged atmospheric profiles from two different atmospheric reanalysis families (i.e. produced either by the European Centre for Medium-Range Weather Forecasts or by the National Oceanic and Atmospheric Administration) for all events (see Aubry et al., 2021). The main IVESPA spreadsheet also contains derived atmospheric parameters, namely the vertically-averaged (between vent and top height) values of Brunt-Väisälä frequency and horizontal wind speed. For this study, we additionally calculate the following derived atmospheric parameters:

- Vertically averaged relative humidity: For each event, we interpolate relative humidity at 1000 regularly spaced altitudes using a piecewise cubic Hermite interpolating polynomial function, after removing non-attributed values for high altitudes for the NOAA reanalyses. We exclude all values at altitudes smaller than the vent height or higher than $\overline{H}_{top}$ (or $\overline{H}_{spr}$ if $\overline{H}_{top}$ is not constrained, or $\overline{H}_{SO2}$ if neither $\overline{H}_{top}$ nor $\overline{H}_{spr}$ are constrained), and calculate the average of remaining values.
- Vertically averaged wind shear ($\overline{\frac{dW}{dz}}$): We first interpolate horizontal wind speed values in the same way as relative humidity. We then calculate the absolute value of the vertical derivative of horizontal wind speed at each height, and calculate the vertically averaged value in the same way as relative humidity. The absolute value of the wind speed derivative with height is used because the magnitude of wind shear controls atmospheric stability and turbulence, and in turn potential impacts on entrainment in the volcanic column.
- Vent-level atmospheric properties: Vent-level atmospheric pressure, temperature and relative humidity are required to calculate the plume buoyancy flux (S5). We simply obtain these by interpolating corresponding atmospheric profiles at vent altitude for each event, using a piecewise cubic Hermite interpolating polynomial function. For atmospheric pressure, we interpolate the logarithm of pressure because pressure varies exponentially with altitude.

All these additional parameters are provided in Table S1. As for all other atmospheric parameters, we use the mean of the values obtained from the two reanalyses as the best estimate, and half of their difference as the uncertainty at 95% confidence level.

S2. Isopleth-based heights

Information on all isopleth-based height H_{iso} collected are provided in Table S2. The comment column summarizes information found in the literature and justifies any choice made in attributing a value to parameters in this table. The IVESPA ID columns shows the identifier of the IVESPA event to which a value of H_{iso} was attributed. When H_{iso} values of distinct units belonging to a single IVESPA event exist, we averaged these values. When a single H_{iso} value encompasses eruption phases that are distinct events in IVESPA, we attributed that same value to all corresponding IVESPA events.

Information on all found $H_{iso,top}$ estimates are reported in comment column of Table S2, but only estimates made using the Carey and Sparks (1986) method were used to constrain values of $H_{iso,top}$ used in our study. This ensures consistency in the isopleth-based height estimates used as more recent methods account more comprehensively for factors influencing the relationship between clast size measurement (used to build isopleth contour) and volcanic column height. For example, in comparison to Carey and Sparks (1986), Rossi et al. (2019) use exact (volcano-specific) atmospheric conditions, account for the effect of wind on plume dynamics, and improve parameterization of particle sedimentation among other advancements.

Isopleth-based height are measured relative to the altitude where the clasts were sampled, which can sometimes span a large range. Consequently, to obtain heights above sea (a.s.l.) and vent (a.v.l.) levels, the average height at which the clasts were sampled is required and reported in Table S2. Information on the average altitude at which clast were sampled is often not reported explicitly in the literature. In such cases, we made a rough estimate of this altitude by combining maps showing sample location, which are more often included in the literature, with topographic maps either included in the source reporting isopleth-based height or from the internet. In a few cases, authors do not report the sampling altitude but provide $H_{iso,top}$ relative to vent level. In

such cases and for convenience, we report a sampling altitude equal to the vent altitude and a plume height above sampling level equal to that above vent level found in the literature. These cases are clearly flagged in the comment column of table 2.

$H_{iso,top}$ uncertainties reported either correspond to uncertainties reported in the literature or assessed from the difference between estimates found in distinct sources (in all cases, using only information related to $H_{iso,top}$ estimates using the method of Carey and Sparks, 1986). In many cases, we could not provide any uncertainty estimates. In comparison to heights reported in IVESPA, $H_{iso,top}$ estimates were often constrained from a single reference, and no more than 2-3. They also did not undergo the same quality-control procedure as key eruption source parameters in IVESPA (i.e., two members of the IVESPA working group independently making estimates based on their own literature search before comparing their values and reaching a consensus). We thus expect that both the $H_{iso,top}$ best estimate and uncertainty are less reliable than other parameters reported in IVESPA.

S3. Scalings relating height and mass eruption rate

In table 1, we calibrate and compare the performance of eight different scalings relating $\overline{H}_{top}$ to the $\overline{MER}$. For four of them, the expressions are fully detailed in Table 1. Here we detail the expressions of the other three (Degruyter and Bonadonna, 2012; Woodhouse et al., 2013; Aubry et al., 2017), which all take the form

$$\overline{H}_{top} = a \times \overline{MER}^{0.25} \times \overline{N}^{-0.75} \times f \quad (S.2)$$

Where f is a function of atmospheric parameters, entrainment parameters and eruption source parameters, and a is a fit parameter.

We use a fit parameter a in equation S.2 instead of the published theoretical pre-factor values for these scalings because they are originally formulated using the plume buoyancy flux instead of $\overline{MER}$ (with these two parameters being proportional), because the prefactors might depend on poorly constrained entrainment coefficient values, and because the scalings were derived under idealized assumptions (e.g. point source, Boussinesq flow) not met for volcanic plumes. Consequently, it is unrealistic to expect theoretical prefactors to be realistic for our study.

In its original form, the Degruyter and Bonadonna (2012) scaling expresses $\overline{MER}$ as a 4th degree polynomial function of $\overline{H}_{top}$. There is no analytical solution for expressing $\overline{H}_{top}$ as a function of $\overline{MER}$ instead, but Aubry et al. (2017) shows that the numerical solution is well approximated (R^2>0.99) by Equation S.2 with:

$$f = f_{DB12} = \frac{1+0.17\frac{\beta^2}{\alpha^{3/2}}V^* + 0.00061\left(\frac{\beta^2}{\alpha^{3/2}}V^*\right)^2}{1+0.48\frac{\beta^2}{\alpha^{3/2}}V^* + 0.0072\left(\frac{\beta^2}{\alpha^{3/2}}V^*\right)^2} \quad (S.3),$$

where β is the wind entrainment coefficient, α is the radial entrainment coefficient, and $V^* = \frac{W}{(FN)^{1/4}}$ with F the plume buoyancy flux, W the vertically averaged wind speed, and N the vertically averaged Brunt Vaisala frequency. Because we only have constraints on $\overline{MER}$ for most

events in IVESPA, we calculate V^* as $\frac{W}{(MER\ N)^{1/4}}$ and f_{DB12} as $\frac{1+0.17b\ V^*+0.00061(b\ V^*)^2}{1+0.48b\ V^*+0.0072(b\ V^*)^2}$ where b is a parameter, proportional to $\frac{\beta^2}{\alpha^{3/2}}$ and to the ratio of the buoyancy flux to the mass eruption rate. We calibrate b as part of the fitting procedure and deem any negative value unphysical.

The Woodhouse et al. (2013) scaling follows Equation S.2 with:

$$f = f_{W13} = \frac{1+\left(0.87+0.5\frac{\beta}{\alpha}\right)W_s}{1+\left(1.09+0.32\frac{\beta}{\alpha}\right)W_s+\left(0.06+0.03\frac{\beta}{\alpha}\right)W_s^2} \quad (S.4)\ ,$$

where $W_s = \frac{1}{\overline{N}}\overline{\frac{dW}{dz}}$. With estimates of α and β ranging between 0.05-0.17 and 0.1-1 respectively (see Aubry et al., 2017, 2018 and references therein), the ratio $\frac{\beta}{\alpha}$ is expected to be between 0.59 and 20, and we deem any calibrated value outside 0.3-40 unphysical in Table 1.

Last, the Aubry et al. (2017) scaling follows Equation S.2 with

$$f = f_{A17} = \frac{1}{\sqrt{1+\frac{\beta}{\alpha}W^*}} \quad (S.5)\ ,$$

where $W^* = \frac{\overline{W}}{U_0}$ with U_0 the column exit velocity at vent level. As for the Woodhouse et al. (2013) scaling, we deem any calibrated value of $\frac{\beta}{\alpha}$ outside 0.3-40 unphysical in Table 1. U_0 is constrained for only 10 events (out of 134) in IVESPA, but the exit water vapor fraction (n_0) and temperature (T_0) are known for 73 and 38 events respectively (Aubry et al., 2021). We thus use the model of Woods and Bower (1995) to calculate the exit velocity as $U_0 = 1.85\sqrt{Rn_0T_0}$ with R the specific gas constant (461.5 J/kg/K). For events with no constraint on n_0 or T_0, we use values of these parameters equal to the average for events for which they are constrained (i.e. 2.7 wt.% for n_0 and 1250 K for T_0).

S4. Scaling calibration, fitness metric and weights

We calibrate all scalings in Table 1 using Matlab non-linear regression model fit function fitnlm (https://uk.mathworks.com/help/stats/fitnlm.html) minimizing the coefficient of determination $\mathbf{R^2 = 1 - \frac{SSE}{SST}}$ with SSE being the sum of squares error and SST the sum of squared total

(adjusted R^2 values, accounting for the number of independent variables in the models, are presented in Table 1). Furthermore, we use weights in SSE and SST calculations e.g.:

$$\mathbf{SSE} = \sum_{\mathbf{i}} \mathbf{w_i} \left(\mathbf{y_i^{pred}} - \mathbf{y_i^{obs}}\right)^{\mathbf{2}} \quad \text{(S.6)}.$$

Where i denotes an IVESPA event, w the value of the weight, y^{pred} the model-predicted value of the dependent variable y and y^{obs} its observed value (in the case of Table 1, y is $\overline{\mathbf{H}}_{\mathbf{top}}$).Weights w are always normalized so that $\sum_{\mathbf{i}} \mathbf{w_i} = \mathbf{1}$, and for simplicity we omit this normalization in the following weight definitions (Equations S.7-S.10).

In column 3 of Table 1 (labeled "none"), there is no weight applied in R^2 calculation i.e.

$$\mathbf{w_i} = \mathbf{1} \quad (\mathbf{S.7}).$$

In column 4 of Table 1 (labeled "eruption"), we give the same weight to each eruption in IVESPA i.e.

$$\mathbf{w_i} = \frac{\mathbf{1}}{\mathbf{n_i}} \quad (\mathbf{S.8}),$$

where n_i is the number of IVESPA events belonging to the same eruption as event i. This prevents eruptions with many events from having disproportionate weights and biasing model calibration and comparison. For example, the Redoubt 1989-1990 eruption has 18 events, representing 14% of the IVESPA events with a top column height estimate.

In column 5 of Table 1 (labeled "uncertainty"), weights are inversely proportional to uncertainties on the difference between the observed and model-predicted height i.e.

$$\frac{\mathbf{1}}{\mathbf{w_i}} = \left(\Delta\overline{\mathbf{H}}_{\mathbf{top}}\right)^{\mathbf{2}} + \left(\mathbf{0.226} \times \frac{\Delta\overline{\mathbf{MER}}}{\overline{\mathbf{MER}}} \times \left(\mathbf{0.3448} \times \overline{\mathbf{MER}}^{\mathbf{0.226}}\right)\right)^{\mathbf{2}} \quad (\mathbf{S.9}),$$

Where $\Delta\overline{\mathbf{H}}_{\mathbf{top}}$ is the uncertainty on the observed top height and the second term is our chosen expression for the squared uncertainty on the scaling-predicted top height. This definition enables less weight to be given to events with higher uncertainty on the observed height and that predicted by scalings from the $\overline{\mathbf{MER}}$. The second term in equation S.9 should be specific to each scaling, e.g. the predicted top height uncertainty will depend on wind uncertainty for the Degruyter and Bonadonna (2012) scaling (Equation S.3), and it should also depend on the final expression of the model calibrated after fitting procedure. However, as we are comparing the different scaling models, the same set of weights should be applied to them all in calculating R^2 values, and prior knowledge of the weights are also needed for model calibration. As a simplification, the second term in Equation S.9 is thus the squared uncertainty on the empirical power-law fit obtained for top height with no weighting (i.e. $\overline{\mathbf{H}}_{\mathbf{top}} = \mathbf{0.3448} \times \overline{\mathbf{MER}}^{\mathbf{0.226}}$) using standard error propagation rules. Simplifying assumptions also had to be made to calculate the error on the $\overline{\mathbf{MER}}$, $\Delta\overline{\mathbf{MER}}$, **using Equation S.1**. Given the different upper and lower bound error on the mass of tephra fallout, we calculate $\Delta\mathbf{M}/\mathbf{M}$ as the mean of relative errors calculated using

the lower and upper bounds. For events with no attributed lower and/or upper bound uncertainty on M, we assume a difference by a factor of 3 between the best estimate and the lower and/or upper bound estimate.

In column 6 of Table 1 (labeled "Flag"), weights are inversely proportional to the sum of the interpretation flags on the best estimates of $\overline{\mathbf{H}}_{\mathbf{top}}$ ($\mathbf{I_H}$) and $\overline{\mathbf{MER}}$ (chosen as the maximum of the interpretation flag on the best estimate of M and D, $\mathbf{I_M}$ and $\mathbf{I_D}$) i.e.

$$\frac{\mathbf{1}}{\mathbf{w_i}} = \mathbf{1} + \mathbf{I_H} + \mathbf{max}(\mathbf{I_M}, \mathbf{I_D}) \quad (\mathbf{S.10}).$$

Weight values in Equation S.10 can thus vary between 0.2 and 1 given interpretation flags take values between 0 (no interpretation) and 2 (significant interpretation). This definition enables less weight to be given to IVESPA events that required significant interpretation to define eruption source parameter values.

In column 7 of Table 1 (labeled "all"), the weights applied are the products of the weights for columns 4-6 (Equations S.8-10), enabling simultaneous application of lower weight to events that belong to the same eruptions, events that have large uncertainty and events that required significant literature interpretation during data collection.

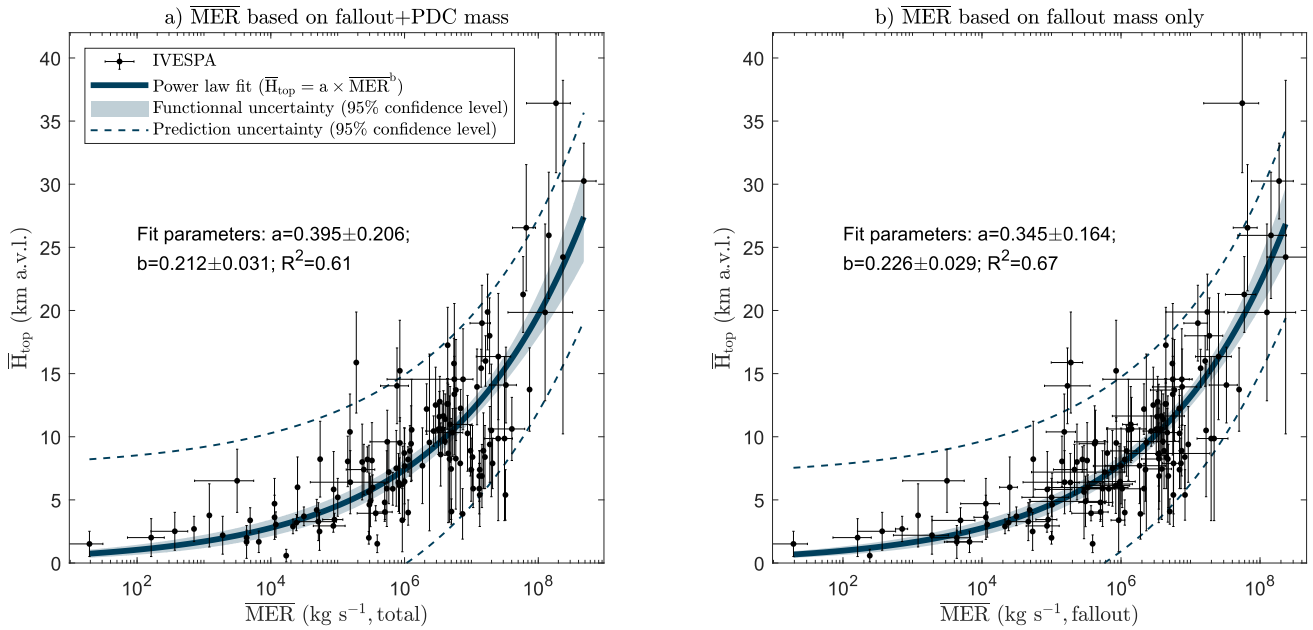

Figure S1. $\overline{\mathbf{H}}_{\mathbf{top}}$ as a function of $\overline{\mathbf{MER}}$ and corresponding power law fit for all IVESPA events with $\overline{\mathbf{MER}}$ as an independent variable. In panel b, the $\overline{\mathbf{MER}}$ is the same as throughout the manuscript i.e. it is calculated using the tephra fallout deposit mass. In panel a, the $\overline{\mathbf{MER}}$ is calculated using the total tephra deposit mass, i.e. the sum of fallout and pyroclastic density current deposits.

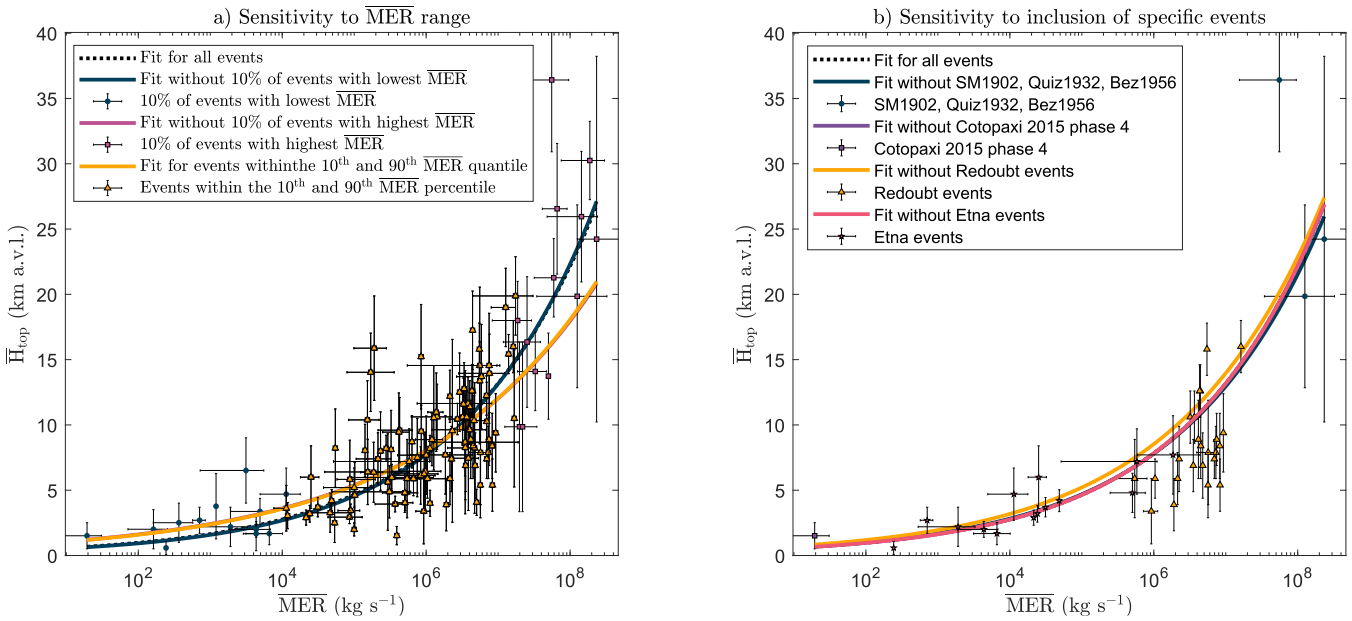

Figure S2. $\overline{\mathbf{H}}_{\mathbf{top}}$ as a function of $\overline{\mathbf{MER}}$ and corresponding power law fits with $\overline{\mathbf{MER}}$ as an independent variable. The black dotted line shows the fit for all events from Figure 1.a. Coloured lines show the fit for specific subgroup of events determined: according to the $\overline{\mathbf{MER}}$ value (a), or excluding events from specific volcanoes or from select high- $\overline{\mathbf{MER}}$ eruptions with high uncertainties on $\overline{\mathbf{H}}_{\mathbf{top}}$ and/or $\overline{\mathbf{MER}}$ (b).

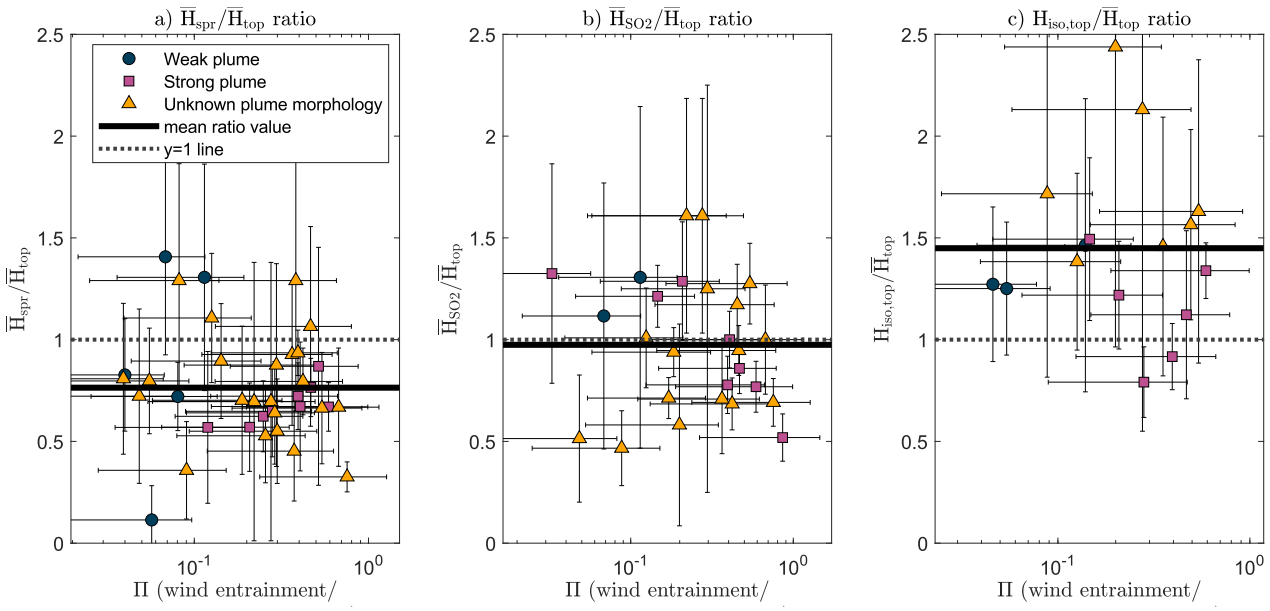

Figure S3. Ratios $\overline{\mathbf{H}}_{\mathbf{spr}}/\overline{\mathbf{H}}_{\mathbf{top}}$ (a), $\overline{\mathbf{H}}_{\mathbf{SO2}}/\overline{\mathbf{H}}_{\mathbf{top}}$ (b), and $\mathbf{H}_{\mathbf{iso,top}}/\overline{\mathbf{H}}_{\mathbf{top}}$ (c) as a function of the Π parameter. The thick horizontal line show the mean ratio value and the dotted line shows the y=1

line. Blue circles, purple squares and yellow triangles correspond to weak, strong and unknown plume morphology.

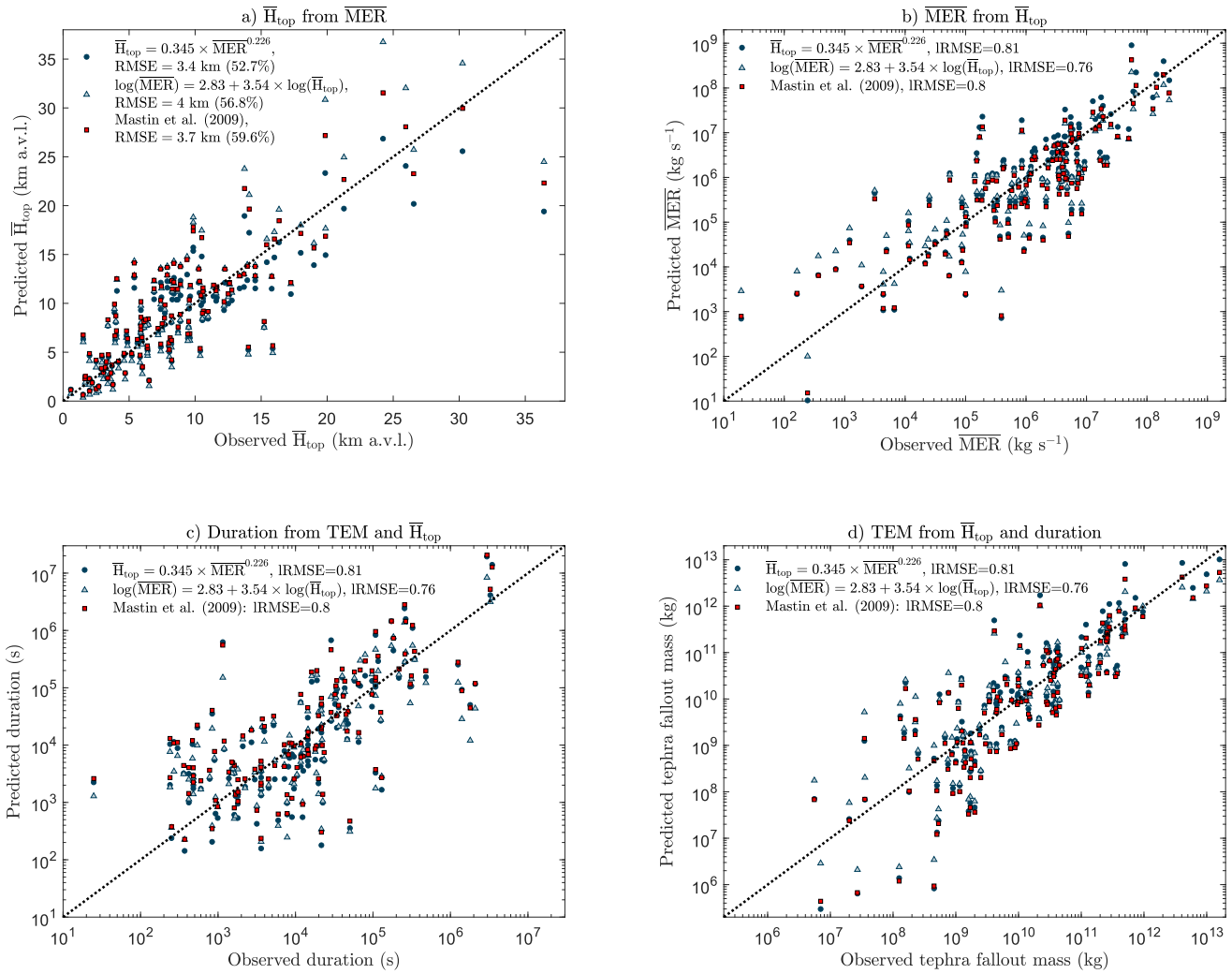

Figure S4. Predicted vs observed $\overline{H}_{top}$ (a), $\overline{MER}$ (b), duration (c) and total erupted mass (TEM) (d) when using our new power law fit (dark blue circles), log-linear fit (light blue triangles) or Mastin et al. (2009) power law fit (red squares) to link $\overline{MER}$ and $\overline{H}_{top}$. Dotted lines show the 1:1 line. Panel a uses the $\overline{MER}$ as the independent variable, whereas panels b-d use $\overline{H}_{top}$ as the independent variable. In panel c, the observed tephra fallout mass is divided by the $\overline{H}_{top}$-derived $\overline{MER}$ to predict duration. In panel d, the $\overline{H}_{top}$-derived $\overline{MER}$ is multiplied by the observed duration to predict tephra fallout mass.

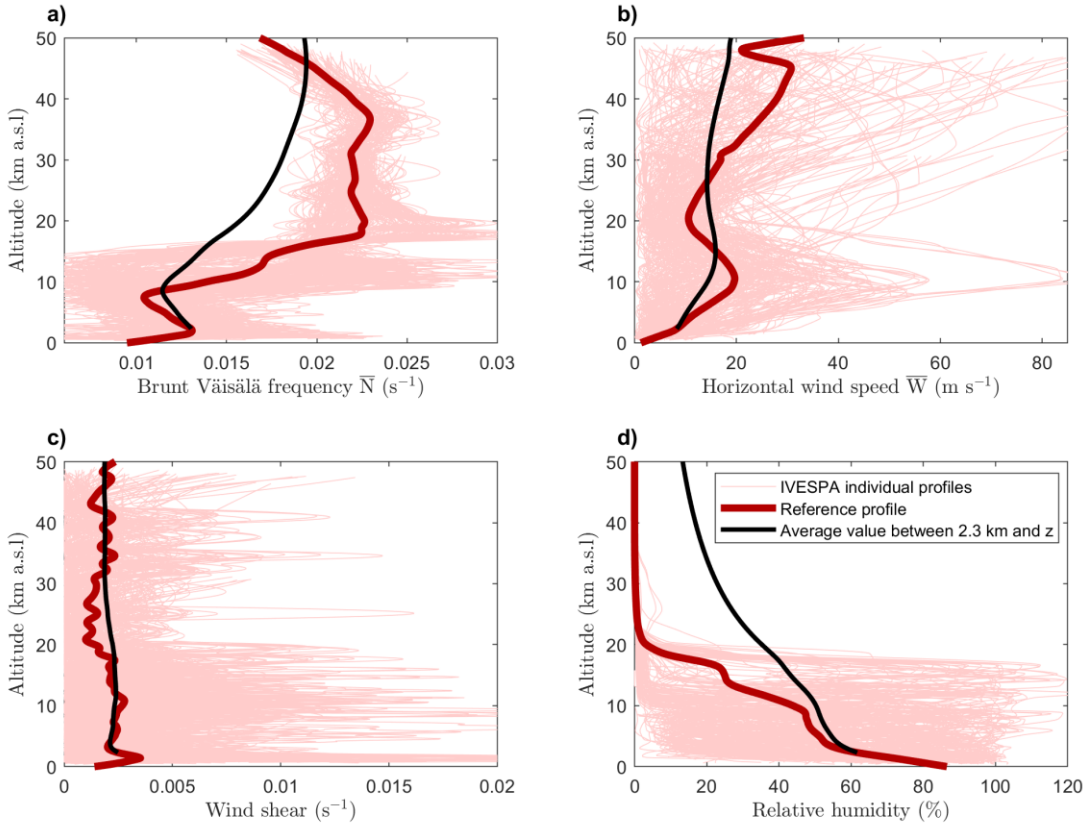

Figure S5. Profiles of Brunt Väisälä frequency (a), horizontal wind speed (b), wind shear (c) and relative humidity (d) for all IVESPA events for both families of atmospheric reanalyses. The thick red line shows the average across all events, smoothed over 2 km, which we refer to as the reference profile. The continuous black line shows the vertically averaged value of the reference profile between 2.3 km (the mean vent altitude in IVESPA) and the altitude shown on the y-axis.

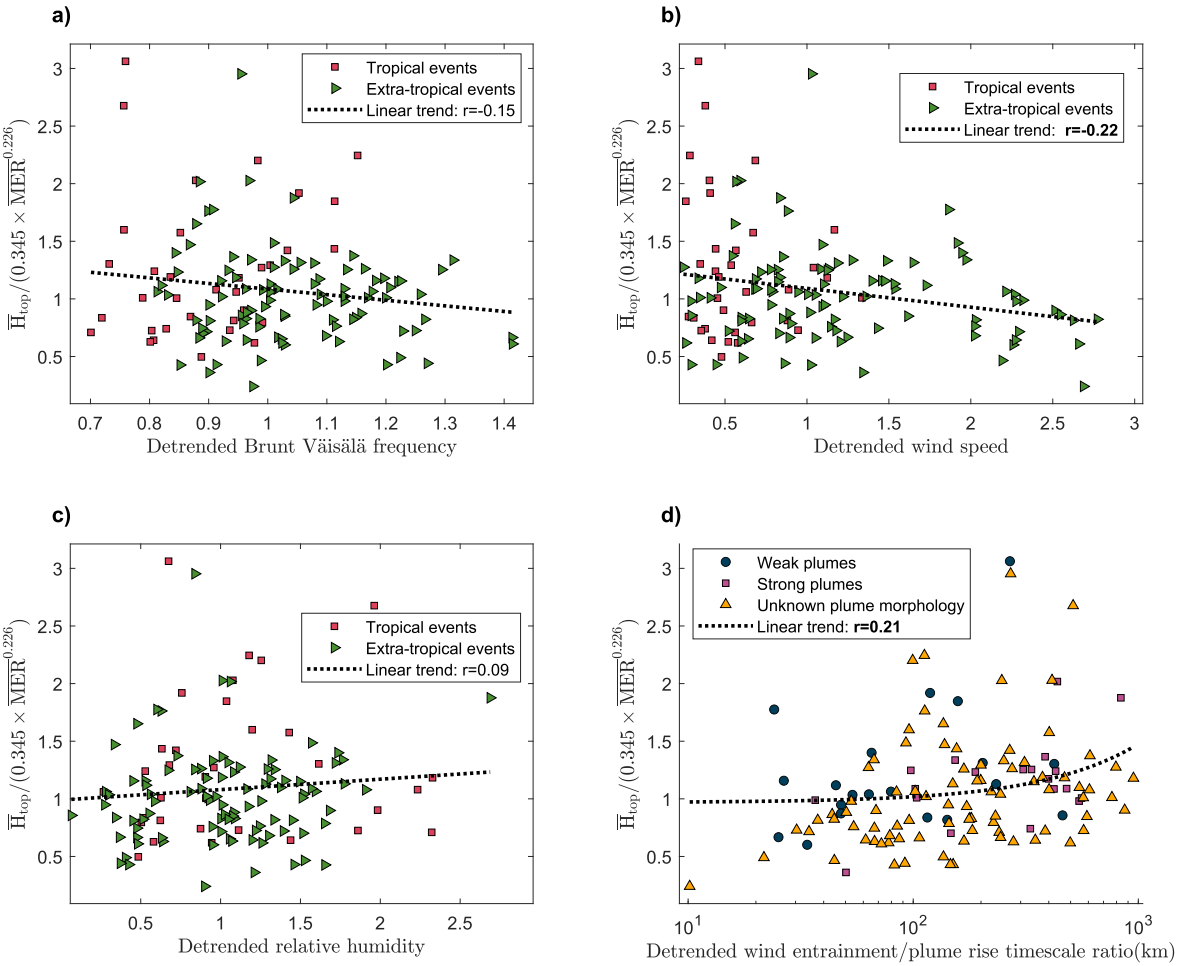

Figure S6. Same as Figure 2, but showing standardized $\overline{H}_{top}$ as a function of detrended atmospheric parameters instead of raw atmospheric parameters. We define detrended atmospheric parameters as the ratio of the vertically averaged value for the considered event to the vertically averaged value for all events, i.e. the vertically averaged value of the reference profile (Figure S5; all vertical averages are between the vent altitude and $\overline{H}_{top}$ specific to the event). Detrended atmospheric conditions thus reflect how vertically averaged conditions deviate from the expected average value for the event vent altitude and $\overline{H}_{top}$, i.e. they should only reflect variations in atmospheric conditions related to the volcano location, eruptive event season, and meteorological variability.

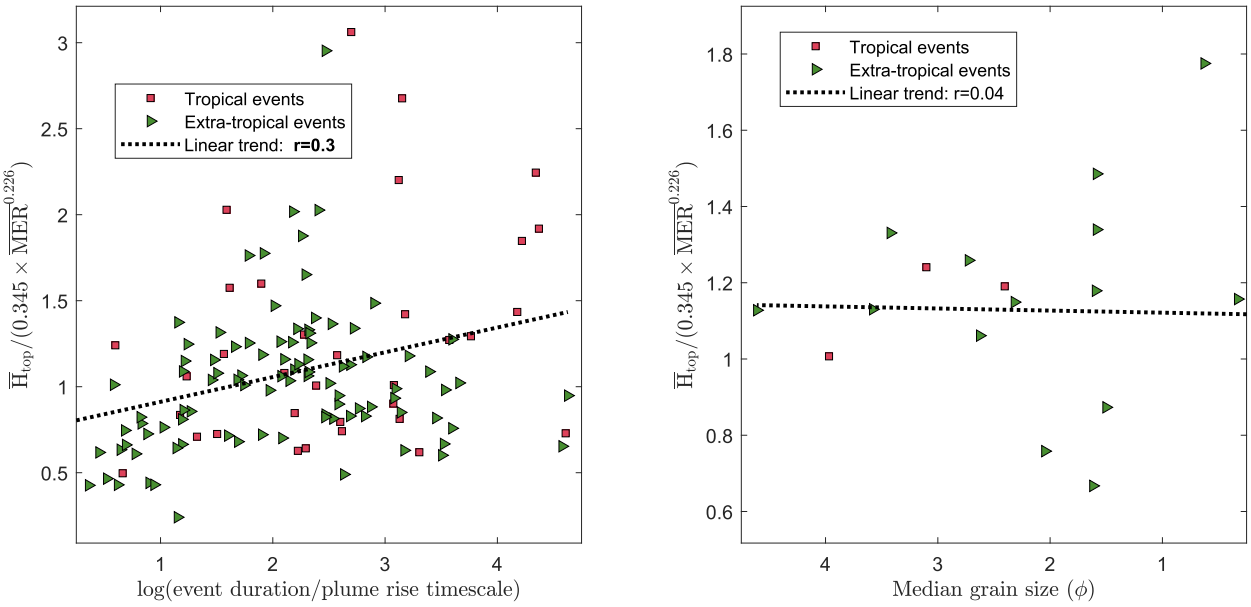

Figure S7. Same as Figure 2, but showing standardized $\overline{H}_{top}$ as a function of the logarithm of the ratio event duration/plume rise timescale (a) and the median grain size from the total grain-size distribution (TGSD) in Φ units (b). The plume rise timescale is defined as $1/\overline{N}$ following buoyant plume rise theory (Morton et al., 1956). Given the grain size diameter d, the grain size in Φ unit is defined as $-\log_2(d)$.